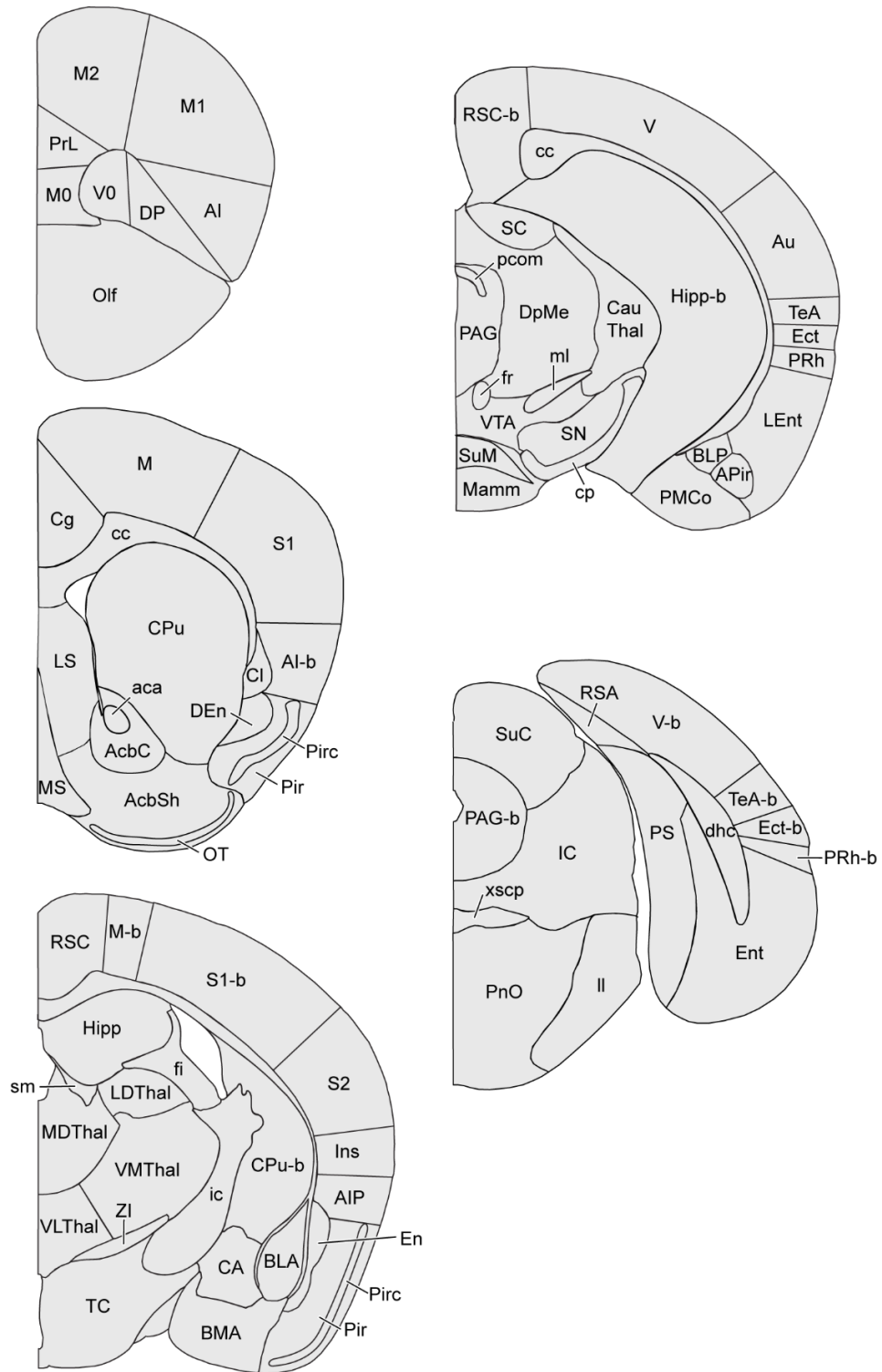


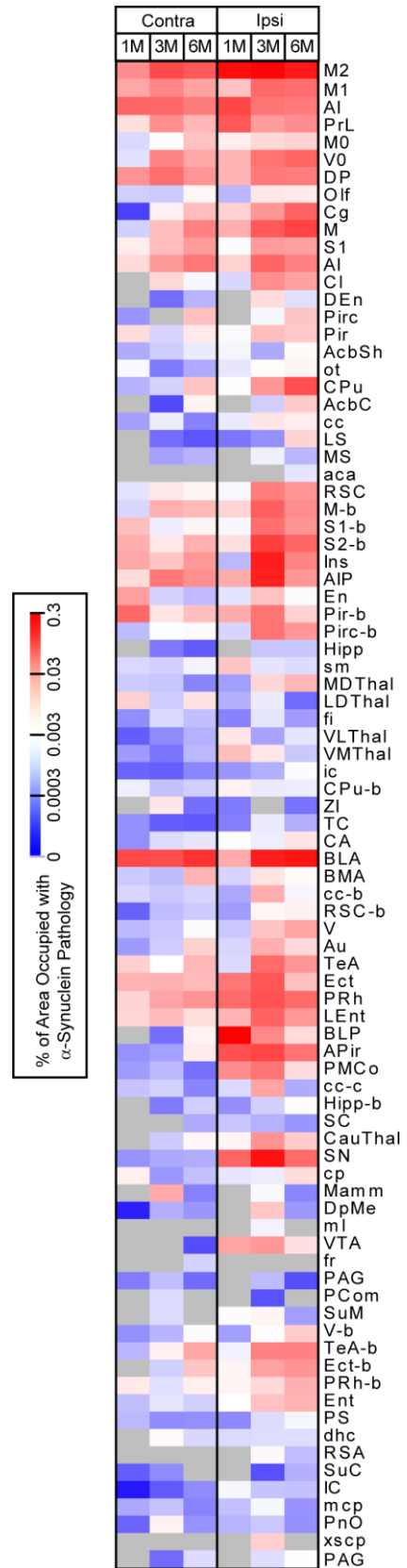
**SUPPLEMENTARY FIGURES**

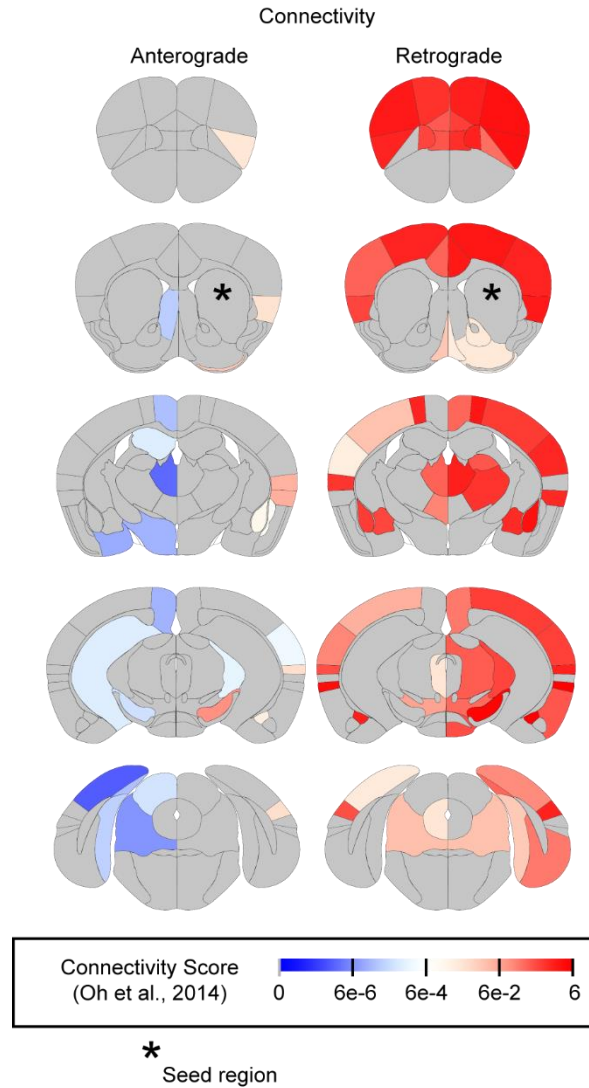


**Supplementary Fig. 1 Analyzed Regions.** The regions annotated for pathology measures and used in subsequent analysis are labeled here as a reference.

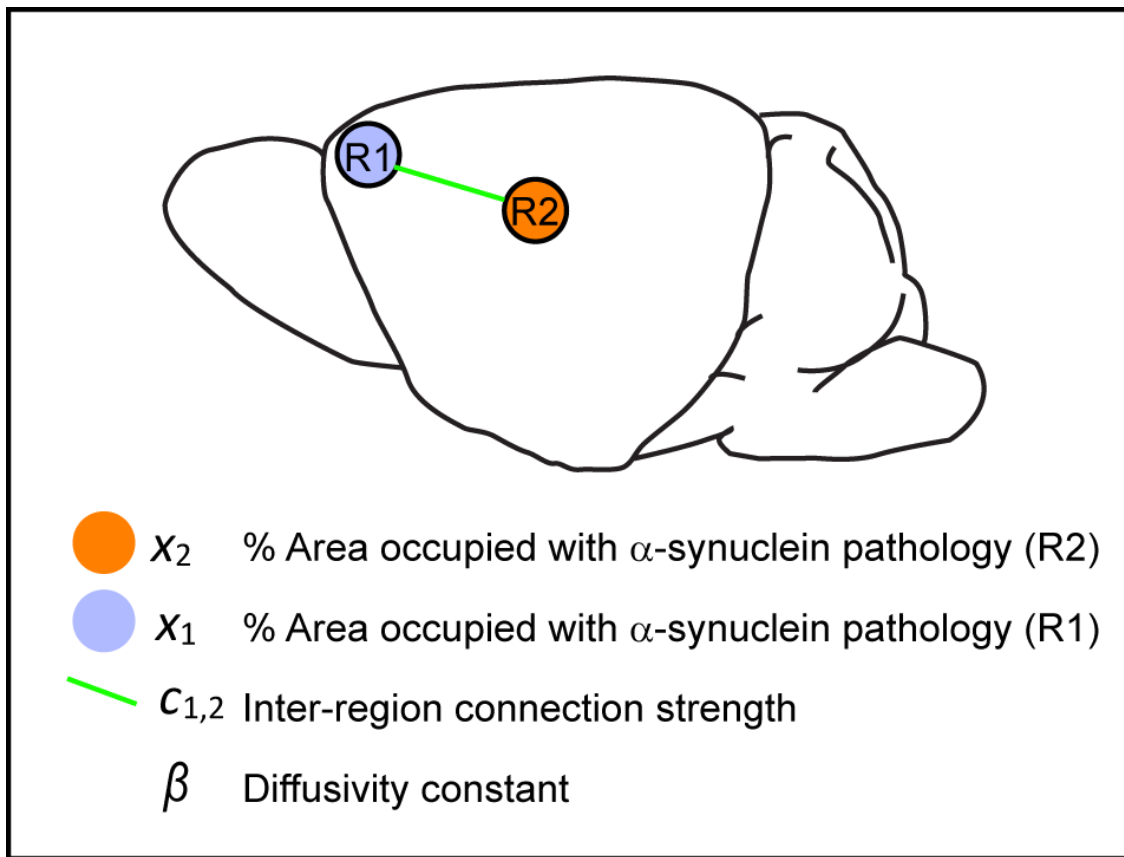
**Supplementary Fig. 2 Heat map of pathological  $\alpha$ -synuclein burden by region and time.**

Pathology in wildtype mice is shown as a log-scale heat map with age post-injection on the x-axis, broken down by contralateral and ipsilateral side, and region of analysis on the y-axis. n (number of mice), 1 MPI=4, 3 MPI=6, 6 MPI=6.



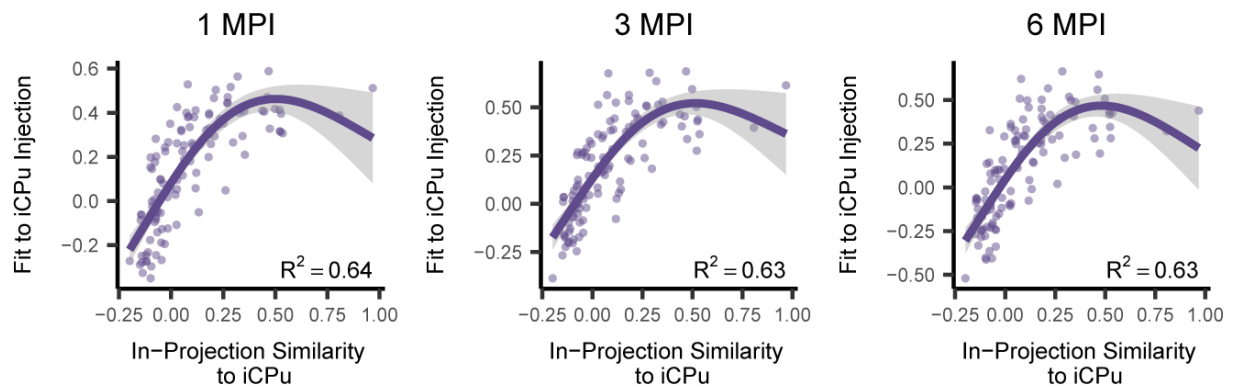


**Supplementary Fig. 3 Heat map representing synaptic connectivity measures to the CPu (from Oh. et al., 2014)** Measures of direct connectivity to and from the CPu as reported in Oh. et al., 2014 are plotted here as a log-scale heatmap. The anterograde connections from the CPu are much weaker, in general, than the retrograde connections to the CPu. Regions in gray have no measure connectivity to or from the CPu.



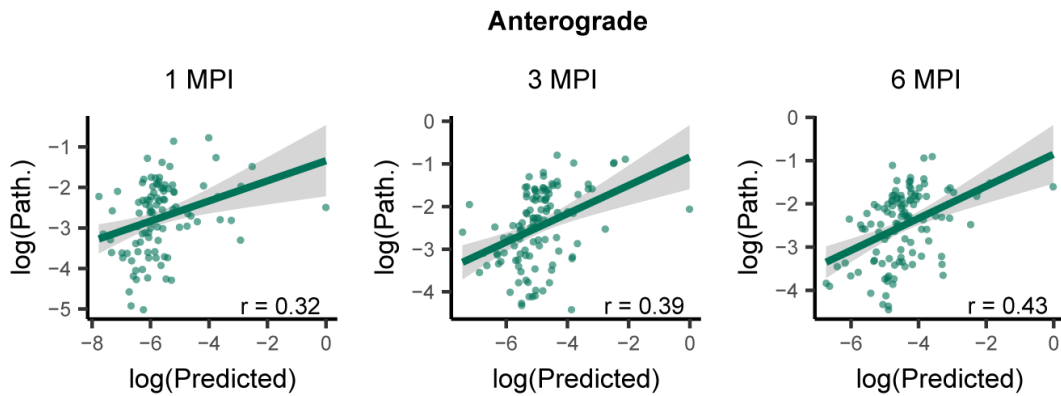
**Supplementary Fig. 4 Concept of a network diffusion model based on anatomical connectivity.**

Network diffusion model paradigm for estimation of pathological protein spread through an anatomically-connected network. Two anatomically-connected regions (R1 and R2) are shown for simplicity, though the network model would incorporate all known anatomical connections. In this case, the amount of pathology in each region ( $x_1$  and  $x_2$ ) and the inter-region connectivity strength ( $c_{1,2}$ ) are known. Therefore, the diffusivity constant ( $\beta$ ) can be used to scale the model to empirical data.

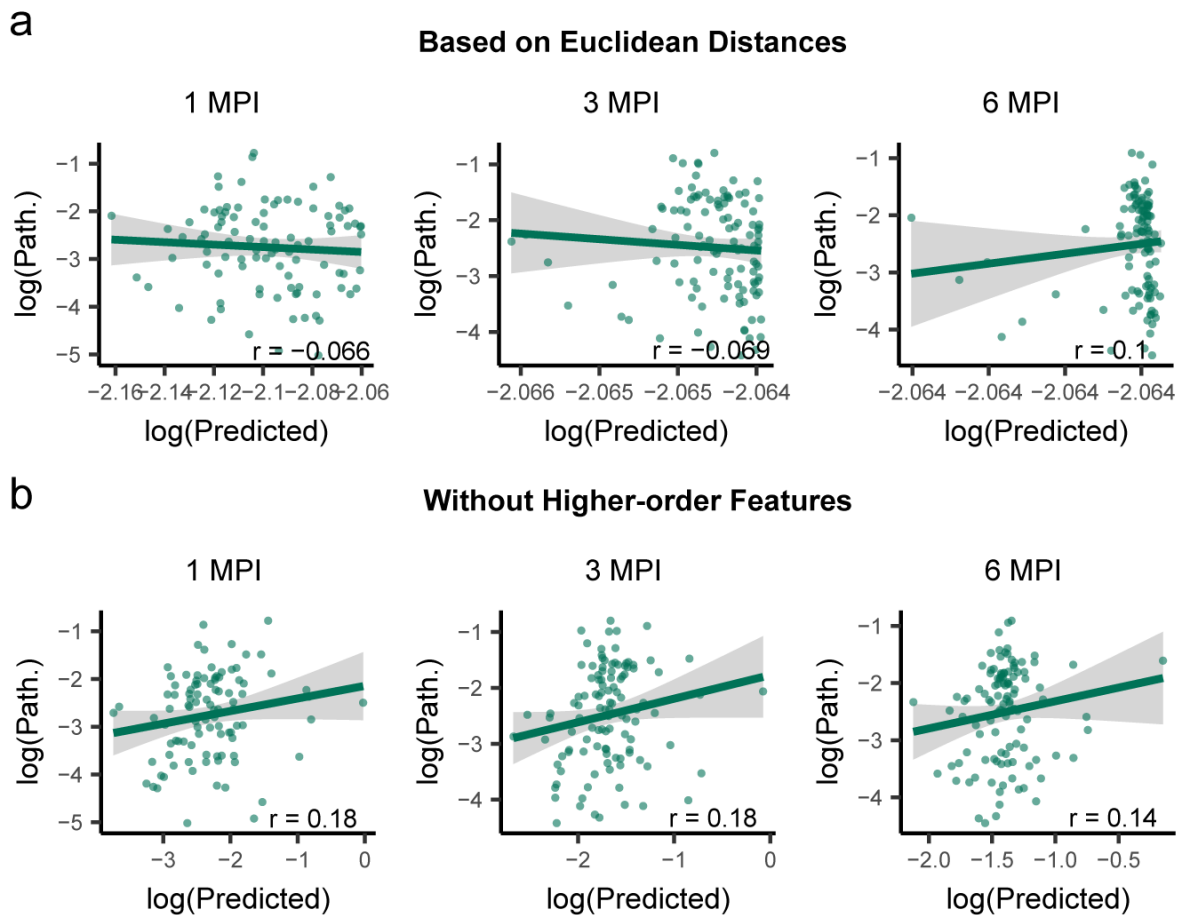


**Supplementary Fig. 5 Fit of alternate seed regions increases with incoming connection profiles more similar to that of iCPu.** We computed the similarity of incoming projections between iCPu and all other regions as the correlation between their respective columns in the synaptic connectivity matrix. We observed a non-linear increase in fit to actual pathological spread from the iCPu when we used alternate seed regions with incoming connections more similar to that of the iCPu. Generalized additive models (GAMs) with incoming connection similarity as smooth terms predicting alternate seed fit are shown for 1 MPI (left panel), 3 MPI (center panel), and 6 MPI (right panel).  $R^2$  values on the plots indicate the amount of variance that the GAM was able to explain in alternate seed fit using in-projection similarity to the iCPu as a predictor variable. The purple line represents the fitted mean and the shaded area is the 95% confidence interval. n (number of mice), 1 MPI=4, 3 MPI=6, 6 MPI=6).

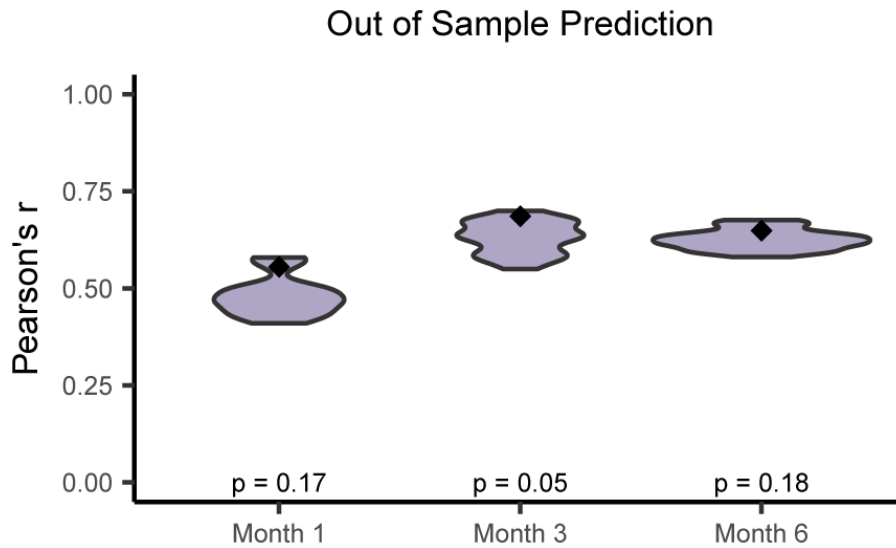
a



**Supplementary Fig. 6 Connectivity-based predictions of anterograde pathological spread from right CPu for NTG and G20 mice.** A network diffusion model based on anterograde spread along synaptic connectivity predicts the spread of pathology over time from a seed in the iCPu. Scatter plots and Pearson correlation coefficients ( $r$ ) between regional  $\log_{10}$ -scaled synuclein pathology values (y-axis) and  $\log_{10}$ -scaled predicted pathology values (x-axis) are shown for month 1 (left panel), month 3 (center panel), and month 6 (right panel). The green line represents the line of best fit, and the shaded ribbon represents the 95% prediction interval. Notably, the anterograde model does not perform as well as the retrograde model.  $n$  (number of mice), 1 MPI=4, 3 MPI=6, 6 MPI=6).

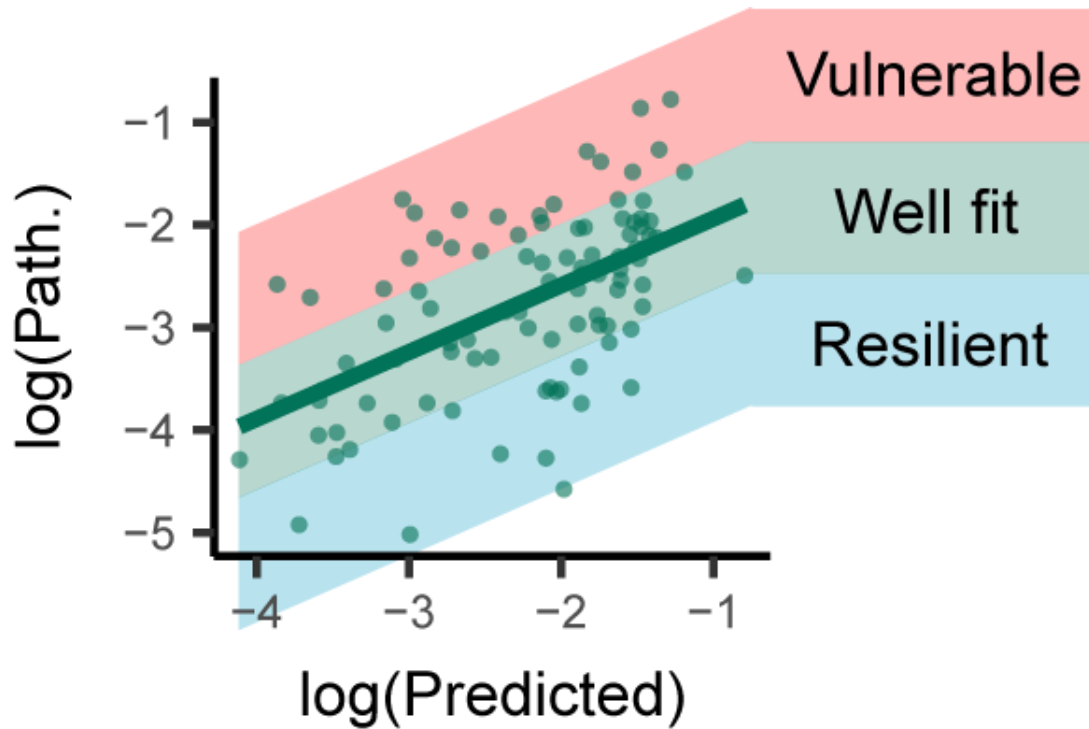


**Supplementary Fig. 7 Distance- and higher-order feature-based predictions of pathological spread from right CPu for NTG mice.** **a**, A network diffusion model based on the Euclidean distances between brain regions poorly explains the observed spread of pathology over time from a seed in the iCPu. Scatter plots and Pearson correlation coefficients ( $r$ ) between regional  $\log_{10}$ -scaled synuclein pathology values (y-axis) and  $\log_{10}$ -scaled predicted pathology values (x-axis) are shown for 1 MPI (left panel), 3 MPI (center panel), and 6 MPI (right panel). The green line represents the line of best fit, and the shaded ribbon represents the 95% prediction interval. **b**, We generated a rewired version of the synaptic connectome that preserved the exact degree sequence while destroying higher order features. This rewired network poorly explains the observed spread of pathology over time from a seed in the iCPu, suggesting that higher order topology of the connectome is a key factor in the model, rather than simple structural properties such as degree. Scatter plots and Pearson correlation coefficients ( $r$ ) between regional  $\log_{10}$ -scaled synuclein pathology values (y-axis) and  $\log_{10}$ -scaled predicted pathology values (x-axis) are shown for 1 MPI (left panel), 3 MPI (center panel), and 6 MPI (right panel). The green line represents the line of best fit, and the shaded ribbon represents the 95% prediction interval.  $n$  (number of mice), 1 MPI=4, 3 MPI=6, 6 MPI=6).



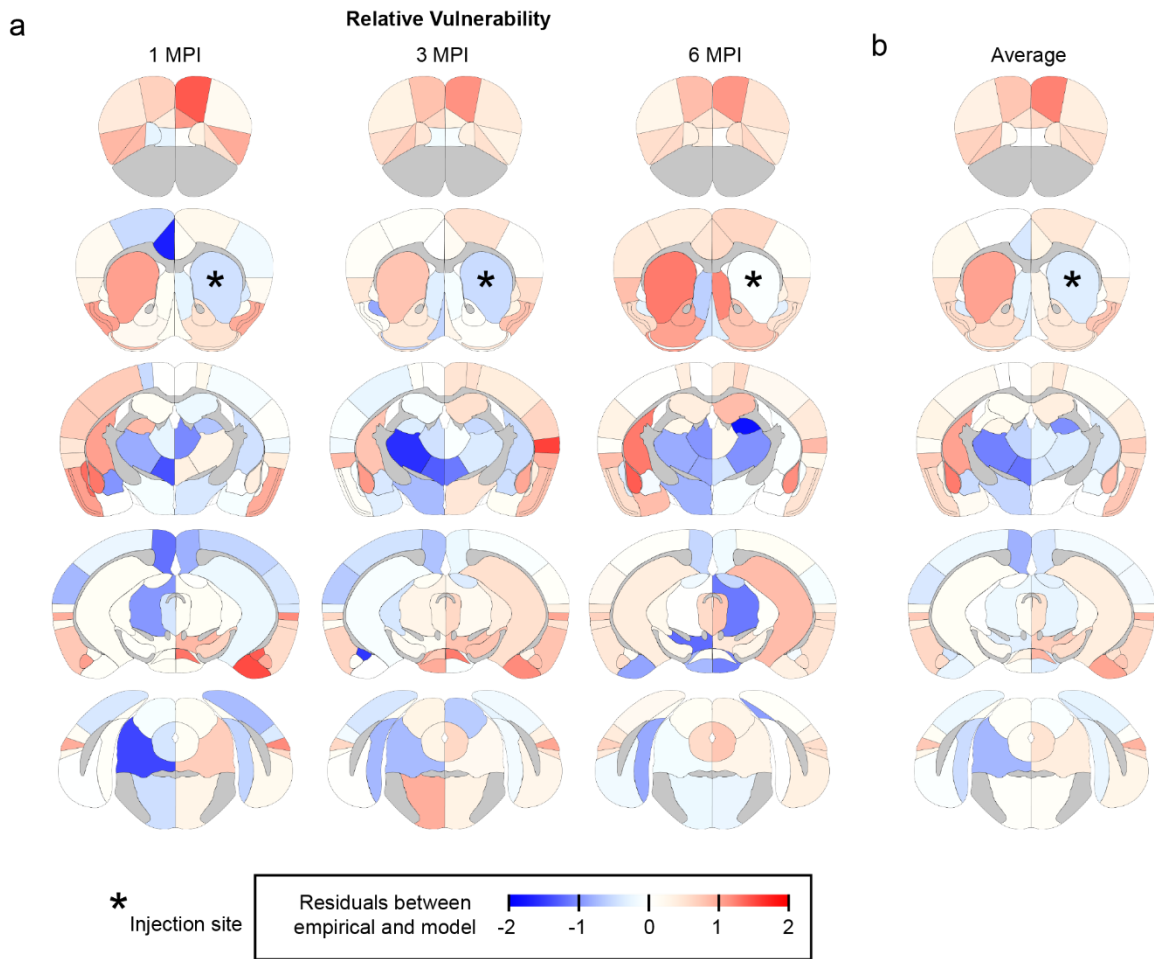
**Supplementary Fig. 8 Split reliability of time constant fit.** For each time point, we randomly sampled half of the mice without replacement and trained the time constant to fit the average of this training sample. Then, we compared the predicted values from the training sample to an average of the remaining mice. This procedure was repeated 100 times to generate a distribution of out-of-sample fits, which were all non-overlapping with 0 and explained considerable amounts of variance (Pearson's  $r > 0.5$  for all out-of-sample predictions at month 3 and month 6). The fits generated by using an average of all mice were at or below the 5<sup>th</sup> percentile of the distribution of out-of-sample fits for all time points. This percentile can also be interpreted as a p-value from a one-tailed, non-parametric test of the null hypothesis that our model is not overfitting the data, such we would observe a fit as high as the fit observed by pooling all the data (black diamond) in a distribution of out-of-sample fits (purple violin plot, width corresponds to observation frequency). We did not correct these p-values for multiple comparisons because we expected not to reject the null hypothesis, and therefore multiple comparisons correction would enforce that finding. Overall, these results suggest a high degree of split reliability for our model in our sample.  $n$  (number of mice), 1 MPI=4, 3 MPI=6, 6 MPI=6.



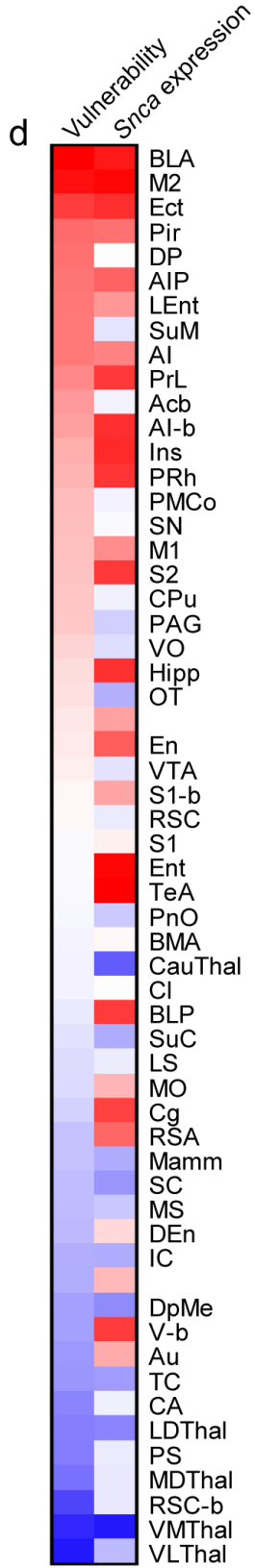
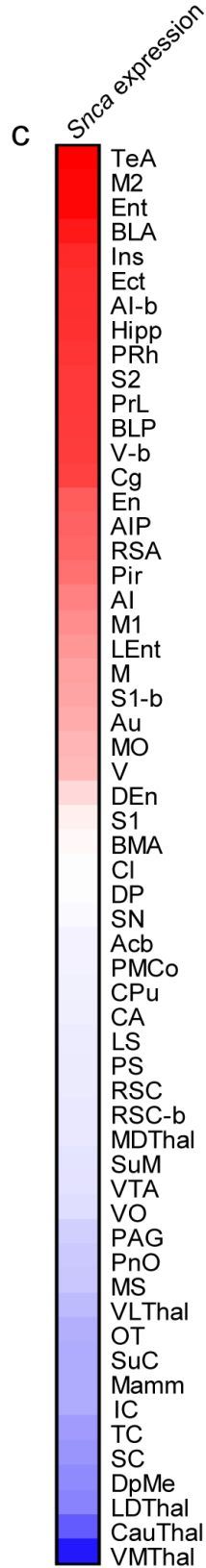
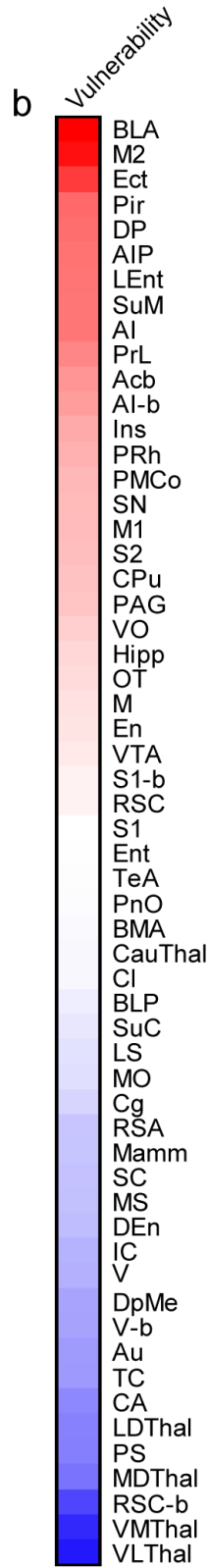
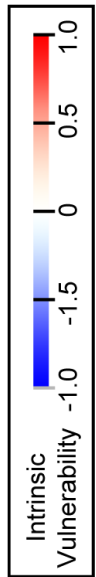
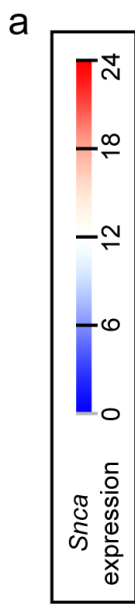


**Supplementary Fig. 9 Conceptual framework for assessment of the relative vulnerability of regions.**

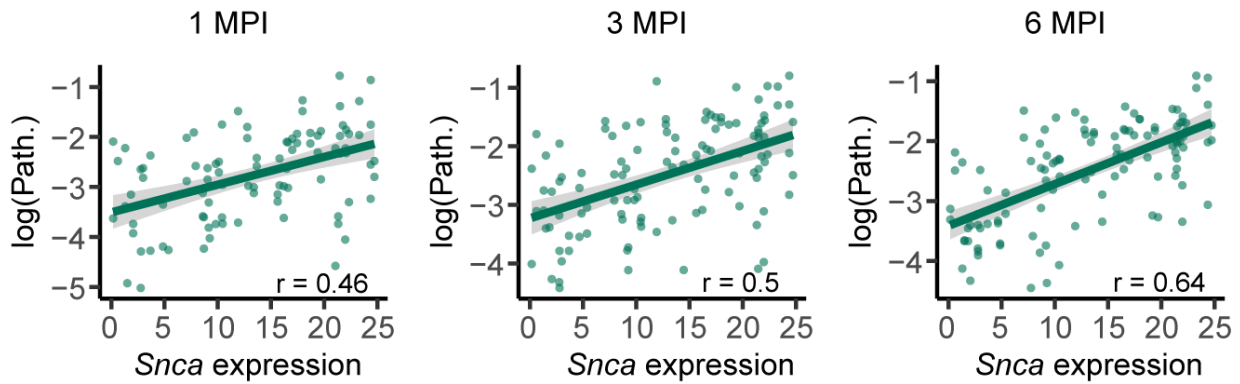
The log predicted pathology vs. log actual pathology graph from 1 MPI is overlaid here with conceptual groups. Most of the regions here are well fit (green shading) by a model which considers only anatomical connectivity. However, regions which have more pathology than expected by connectivity alone are considered relatively vulnerable (red shading), while the regions that have less pathology than would be expected are relatively resilient (blue shading) to pathology induction.



**Supplementary Fig. 10 Using model vs. empirical data residuals to understand vulnerability.** **a**, In order to measure the relative vulnerability of all regions, the residual between pathology predicted based on anatomical connectivity and empirical pathology measures were taken at all timepoints and are displayed as a heat map. **b**, Some of this differential vulnerability can be explained by the difference in the ability to fit pathological data at different timepoints. These differences can be partially abrogated by taking the average residual across timepoints and is reported as the average of the residuals for each region.

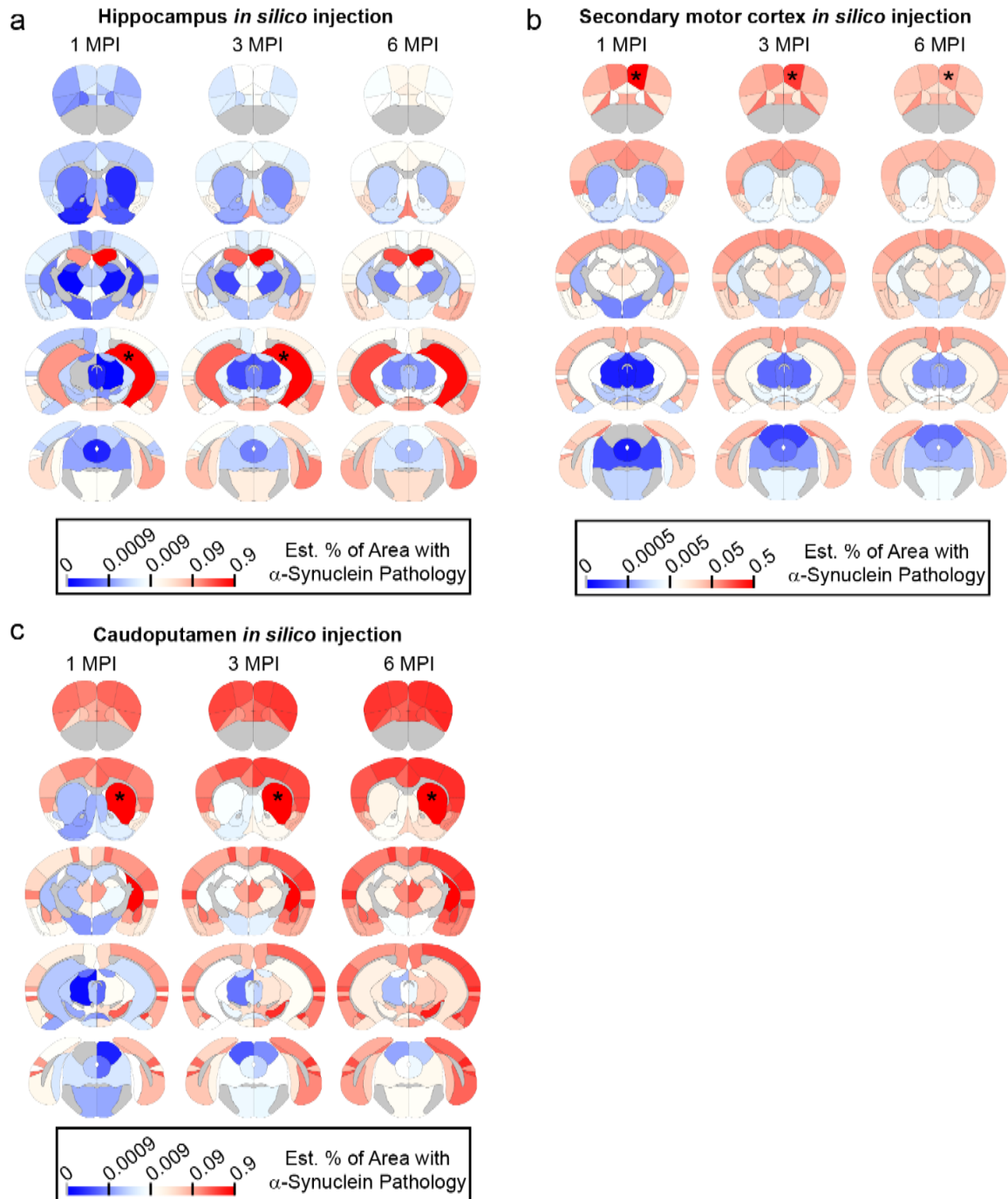


**Supplementary Fig. 11 Computed intrinsic vulnerability and *Snca* gene expression.** **a**, Scale bars for vulnerability and *Snca* expression measures. **b**, Evaluated regions are ranked here from most to least vulnerable based on the fit to modeled pathological  $\alpha$ -synuclein spread as described in the main text. Midbrain and thalamic nuclei are least vulnerable, while select cortical regions and the amygdala show the highest vulnerability. **c**, *Snca* gene expression data from Allen Brain Atlas *in situ* hybridization for the same regions is displayed here from highest expression to lowest expression. The *Snca* gene expression has an overall similar pattern to computed vulnerability, with thalamic and midbrain regions showing the lowest expression, while select cortical regions have the highest *Snca* expression. Note that there are more regions with high *Snca* expression. **d**, Vulnerability and *Snca* expression values displayed side-by-side and sorted by region such that vulnerability and *Snca* expression can be directly compared.

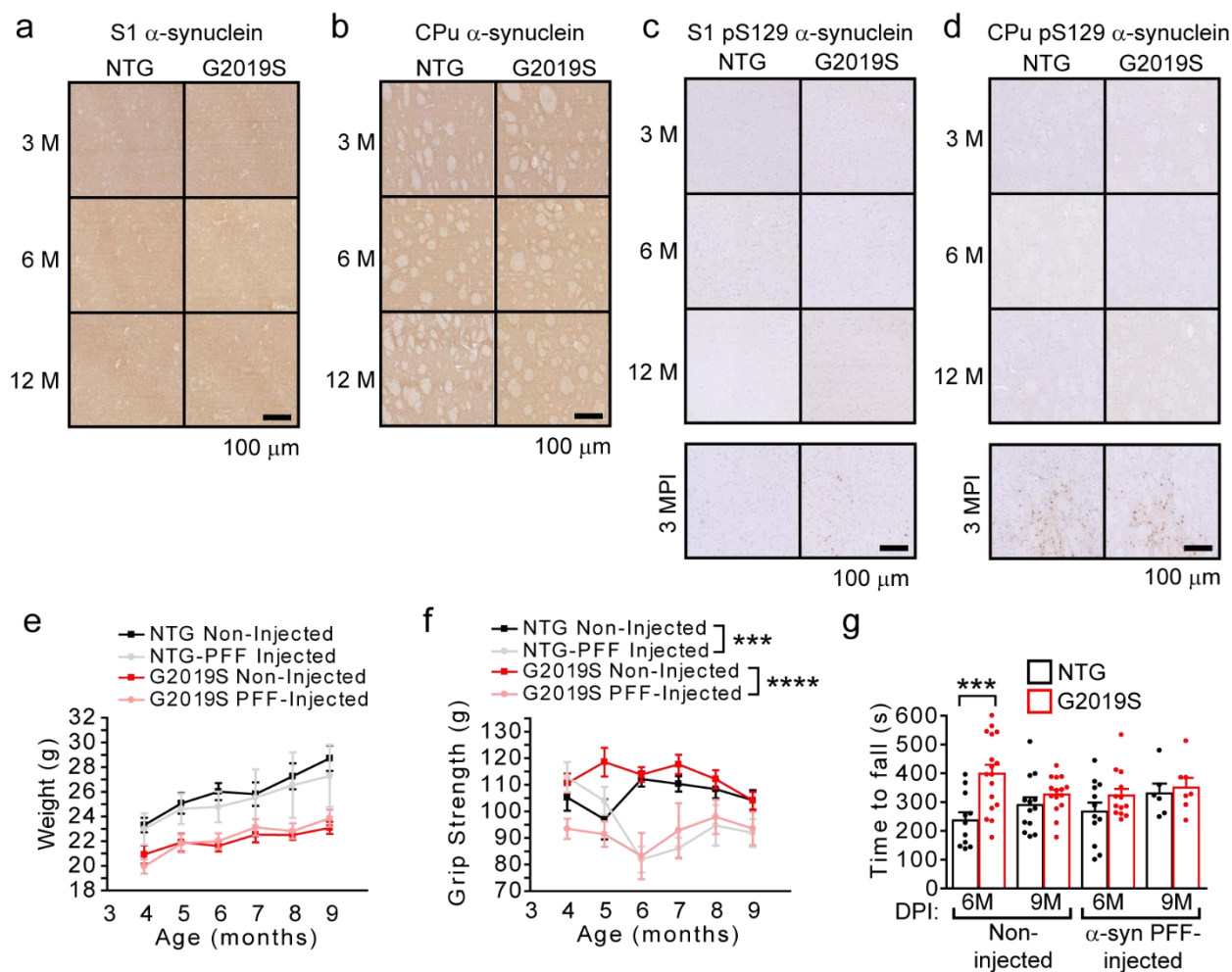


**Supplementary Fig. 12 Correlation of *Sncα* expression with  $\alpha$ -synuclein pathology in NTG mice.**

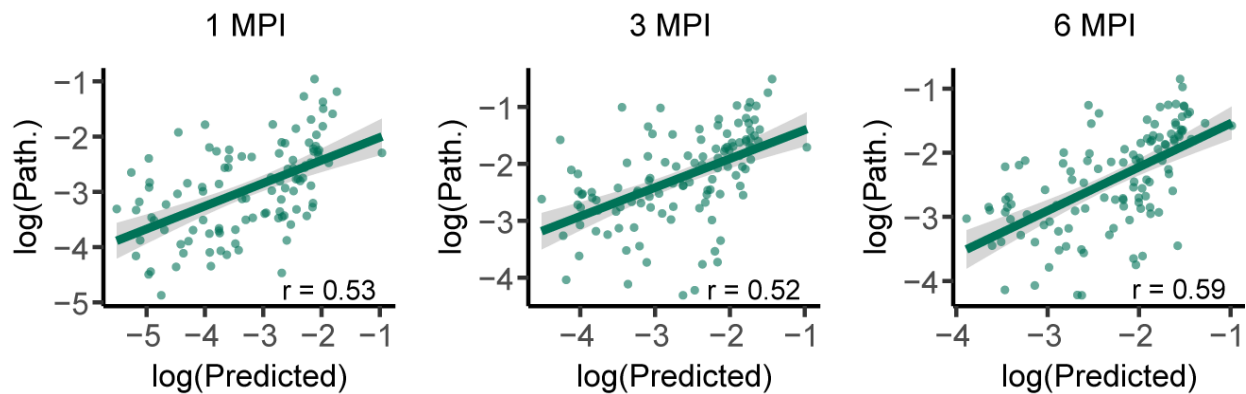
Scatterplots and Pearson correlation coefficients ( $r$ ) of *Sncα* expression versus actual pathology values for each region are plotted for 1 ( $df = 95$ ,  $p_{corr} = 5.92 \times 10^{-6}$ ), 3 ( $df = 111$ ,  $p_{corr} = 7.49 \times 10^{-8}$ ) and 6 ( $df = 111$ ,  $t = 8.70$ ,  $p_{corr} = 1.03 \times 10^{-13}$ ) MPI (two-tailed t-tests). p-Values were Bonferroni-corrected over the 3 time points. The green line represents the line of best fit, and the shaded ribbon represents the 95% prediction interval. n (number of mice), 1 MPI=4, 3 MPI=6, 6 MPI=6.



**Supplementary Fig. 13 *In silico* seeding of alternate regions in mouse brain.** Heat map of regions affected with  $\alpha$ -synuclein pathology with *in silico* propagation of  $\alpha$ -synuclein pathology after seeding in either the **a**, hippocampus, **b**, secondary motor cortex or **c**, caudoputamen. The color scale represents log-transformed mean percentage area occupied with  $\alpha$ -synuclein pathology.

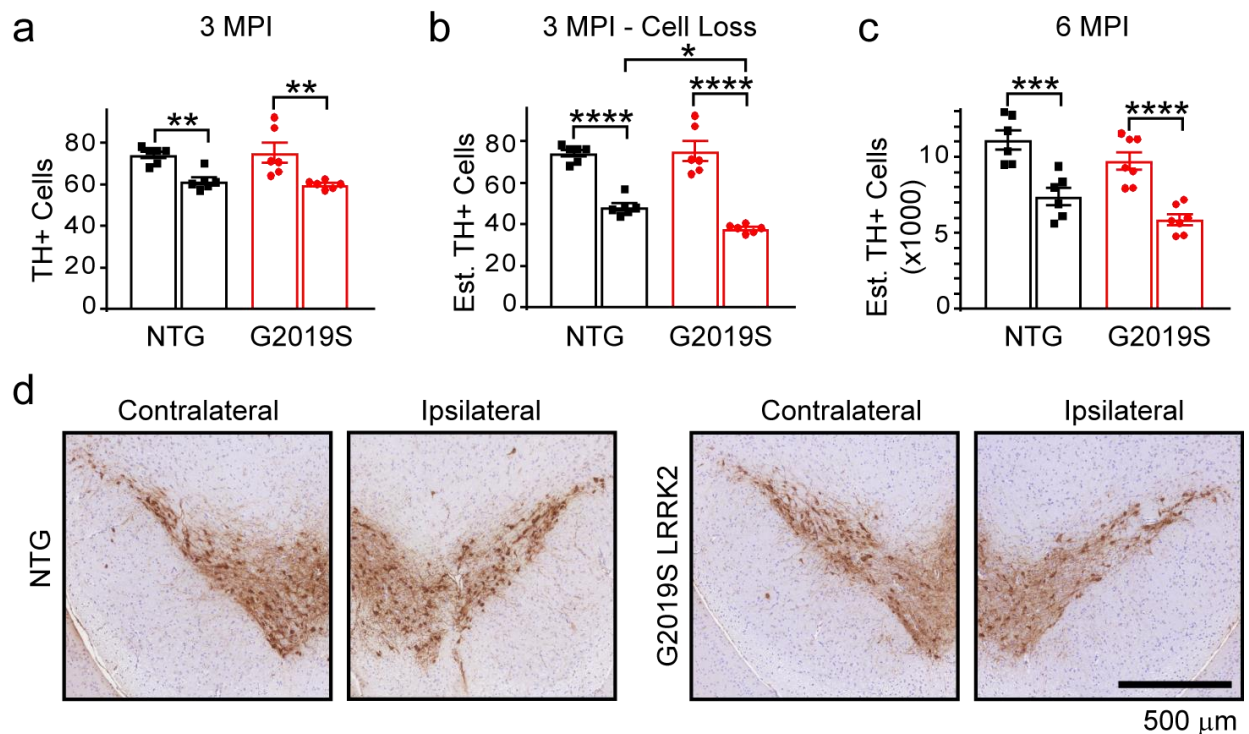


**Supplementary Fig. 14 Characterization of G2019S LRRK2 mice.** G2019S mice have similar  $\alpha$ -synuclein levels and do not accumulate pS129  $\alpha$ -synuclein without the injection of exogenous  $\alpha$ -synuclein PFFs.  $\alpha$ -synuclein staining in the primary somatosensory cortex **a**, and caudoputamen **b**, is similar between NTG and G2019S mice at 3, 6 and 12 months of age ( $n = 3$  mice/age/genotype). Pathological pS129  $\alpha$ -synuclein also does not accumulate in the brains of these mice. Somatosensory cortex **c**, and caudoputamen **d** ( $n = 3$  mice/age/genotype), are shown as compared to mice of the same genotypes 3 months post-injection with  $\alpha$ -synuclein PFFs (bottom). **e**, G2019S mice weigh less than their NTG counterparts on average, and injection with  $\alpha$ -synuclein PFFs does not change this difference. **f**, Grip strength is diminished upon  $\alpha$ -synuclein PFF injection in both genotypes (two-way ANOVA, \*\*\* $p=0.0006$ , \*\*\*\* $p<0.0001$ ), but minimal difference is observed in the response of each genotype. **g**, Non-injected 6-month G2019S mice show an increased latency to fall on the rotarod (two-way ANOVA, \*\*\* $p=0.0006$ ), but this difference is lost by 9 months of age. In contrast, there is no difference between  $\alpha$ -synuclein PFF-injected mice at either 6 months (3 MPI) or 9 months (6 MPI). Scale bars = 100  $\mu$ m. Plots display mean  $\pm$  standard error.  $n$  (number of mice), NTG Non-Injected (4M=14, 5M=10, 6M=12, 7M=11, 8M=11, 9M=16), G2019S Non-injected (4M=12, 5M=15, 6M=15, 7M=16, 8M=15, 9M=17), NTG PFF-Injected (4M=11, 5M=11, 6M=11, 7M=6, 8M=6, 9M=6), G2019S PFF-Injected (4M=12, 5M=9, 6M=9, 7M=7, 8M=7, 9M=7).



**Supplemental Fig. 15 Network diffusion model based on anatomical connectivity explains pathological  $\alpha$ -synuclein spread in G2019S mice.** a, Scatterplots and Pearson correlation coefficients ( $r$ ) of log predicted pathology based on anatomical connectivity versus actual pathology values for each region are shown for 1 ( $df = 104$ ,  $p_{corr} = 1.66 \times 10^{-8}$ ), 3 ( $df = 112$ ,  $p_{corr} = 1.21 \times 10^{-9}$ ) and 6 ( $df = 113$ ,  $p_{corr} = 1.04 \times 10^{-11}$ ) MPI (two-tailed t-tests). p-values were Bonferroni-corrected over the 3 time points. The green line represents the line of best fit, and the shaded ribbon represents the 95% prediction interval. n (number of mice), 1 MPI=6, 3 MPI=6, 6 MPI=7.





**Supplementary Fig. 16 Neuron loss estimate is confirmed in the midbrain by tyrosine hydroxylase counts.** **a**, One section in between the two sections used for pathology quantitation was stained with an anti-TH antibody and used for quantification of substantia nigra neurons in each 3 month post-injection mouse (two-way ANOVA with Sidak's multiple comparison test, \*\* $p=0.0075$  for NTG, \*\* $p=0.0013$  for G2019S). **b**, The mean estimated neuron loss between 3 and 6 months from the SN was subtracted from the TH cell counts in 3 MPI mice (two-way ANOVA with Sidak's multiple comparison test, \*\*\*\* $p<0.0001$  for both NTG and G2019S comparisons, \* $p=0.0135$  for NTG-G2019S ipsilateral comparisons). **c**, Every 10<sup>th</sup> section through the SN was stained with an anti-TH antibody and SN neurons were counted to estimate the total number of neurons present in NTG and G2019S mice 6 months after injection (two-way ANOVA with Sidak's multiple comparison test, \*\*\* $p=0.0002$ , \*\*\*\* $p<0.0001$ ). **d**, Representative images of the contralateral and ipsilateral substantia nigra from NTG and G2019S mice 6 months post-injection (scale bar = 500  $\mu$ m). Plots display mean  $\pm$  standard error with individual values plotted. n (number of mice), 3 MPI-NTG=6, 3 MPI-G2019S=6, 6 MPI-NTG=6, 6 MPI-G2019S=7.

**Supplementary Fig. 17 Representative pathology images from all quantified regions pS129  $\alpha$ -synuclein (EP1536Y) staining (scale bars = 100  $\mu$ m). See Supplementary Fig. 1 for region designations (“i” precedes ipsilateral regions and “c” precedes contralateral regions).**

	1 Month post-injection		3 Months post-injection		6 Months post-injection	
	NTG	G2019S	NTG	G2019S	NTG	G2019S
iM2						
iM1						
iAl						
iPrL						
iM0						
iV0						
iDP						
iOf						

100  $\mu$ m

	1 Month post-injection		3 Months post-injection		6 Months post-injection	
	NTG	G2019S	NTG	G2019S	NTG	G2019S
cM2						
cM1						
cAl						
cPrL						
cM0						
cV0						
cDP						
cOlf						

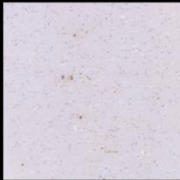
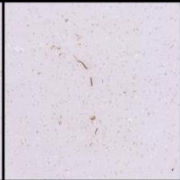
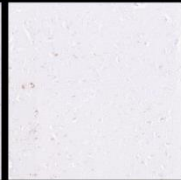
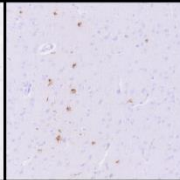
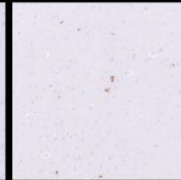
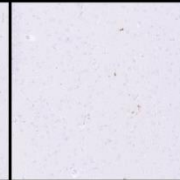
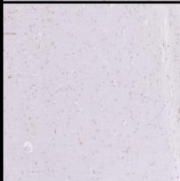



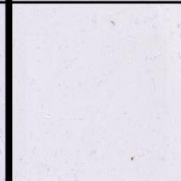
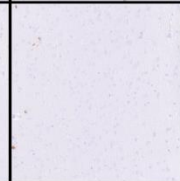

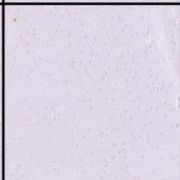


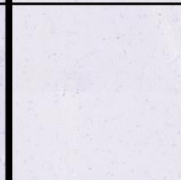
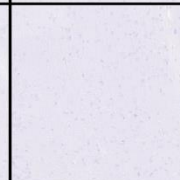
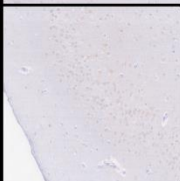

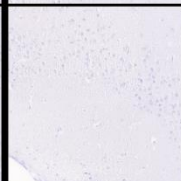


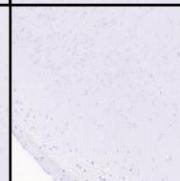
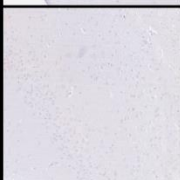
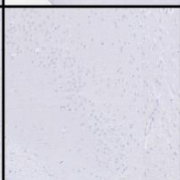
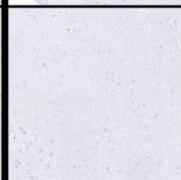
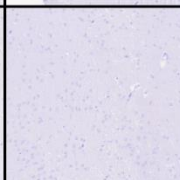
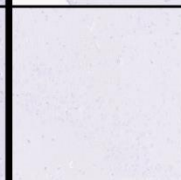
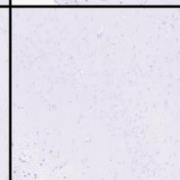

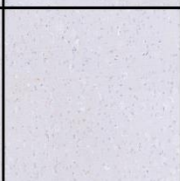
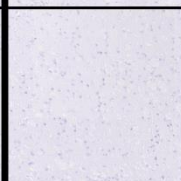
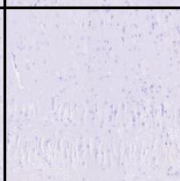
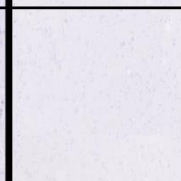
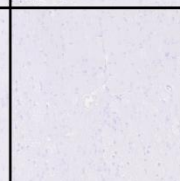
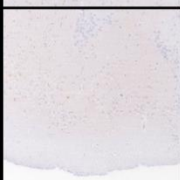
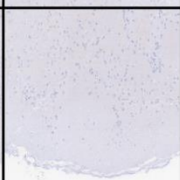
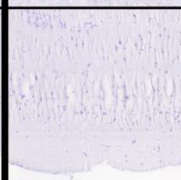
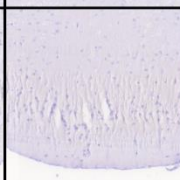
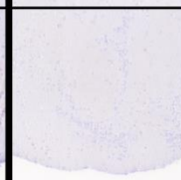



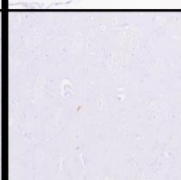


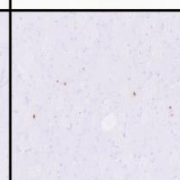
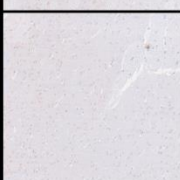

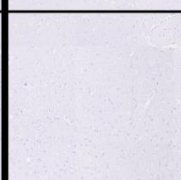
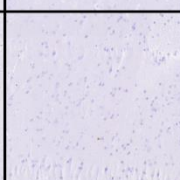
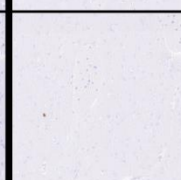
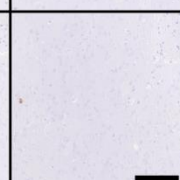
100 μm

	1 Month post-injection		3 Months post-injection		6 Months post-injection	
	NTG	G2019S	NTG	G2019S	NTG	G2019S
iCg						
iM						
iS1						
iS2						
iCl						
iDEn						
iPirc						
iPir						
iAcbSh						

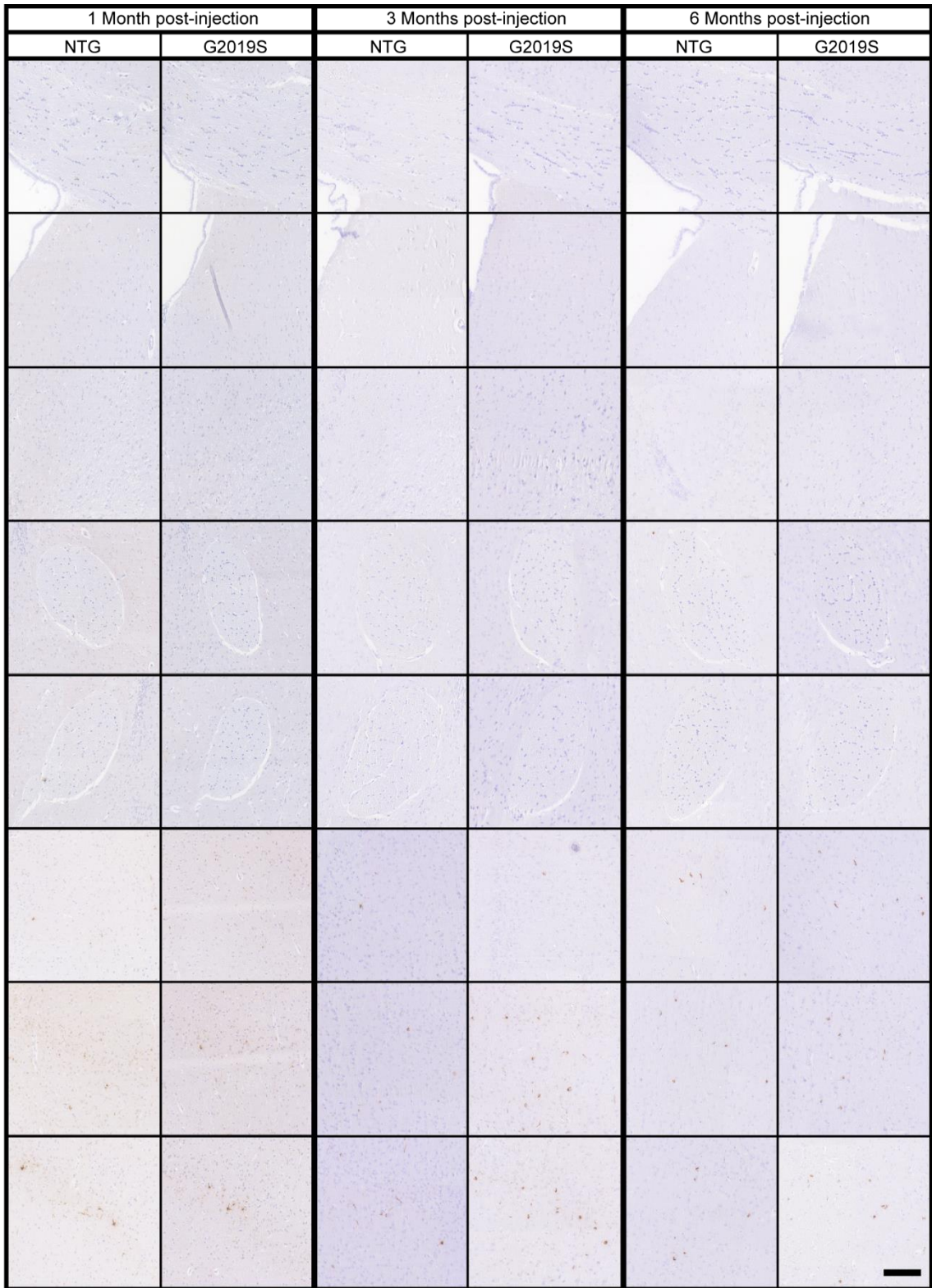
100 μm

	1 Month post-injection		3 Months post-injection		6 Months post-injection	
	NTG	G2019S	NTG	G2019S	NTG	G2019S
iOT						
iCPu						
iAcbC						
icc						
iLS						
iMS						
cCg						
cM						
cS1						

100 μm

	1 Month post-injection		3 Months post-injection		6 Months post-injection	
	NTG	G2019S	NTG	G2019S	NTG	G2019S
cS2						
cCl						
cDEn						
cPirc						
cPir						
cAcbSh						
cOT						
cCPu						
cAcbC						

100  $\mu$ m



100 μm

	1 Month post-injection		3 Months post-injection		6 Months post-injection	
	NTG	G2019S	NTG	G2019S	NTG	G2019S
iS2-b						
iIns						
iAIP						
iEn						
iPir-b						
iPirC-b						
iHipp						
ism						
iMDThal						

100 μm



	1 Month post-injection		3 Months post-injection		6 Months post-injection	
	NTG	G2019S	NTG	G2019S	NTG	G2019S
iLDThal						
ifi						
iVLThal						
iVMThal						
iic						
iCPu-b						
iZI						
iTC						
iCA						

100 μm

	1 Month post-injection		3 Months post-injection		6 Months post-injection	
	NTG	G2019S	NTG	G2019S	NTG	G2019S
iBLA						
iBMA						
cRSC						
cM-b						
cS1-b						
cS2-b						
clns						
cAIP						

100 μm

	1 Month post-injection		3 Months post-injection		6 Months post-injection	
	NTG	G2019S	NTG	G2019S	NTG	G2019S
cEn						
cPir-b						
cPirc-b						
cHipp						
csm						
cMDThal						
cLDThal						
cfi						
cVLThal						

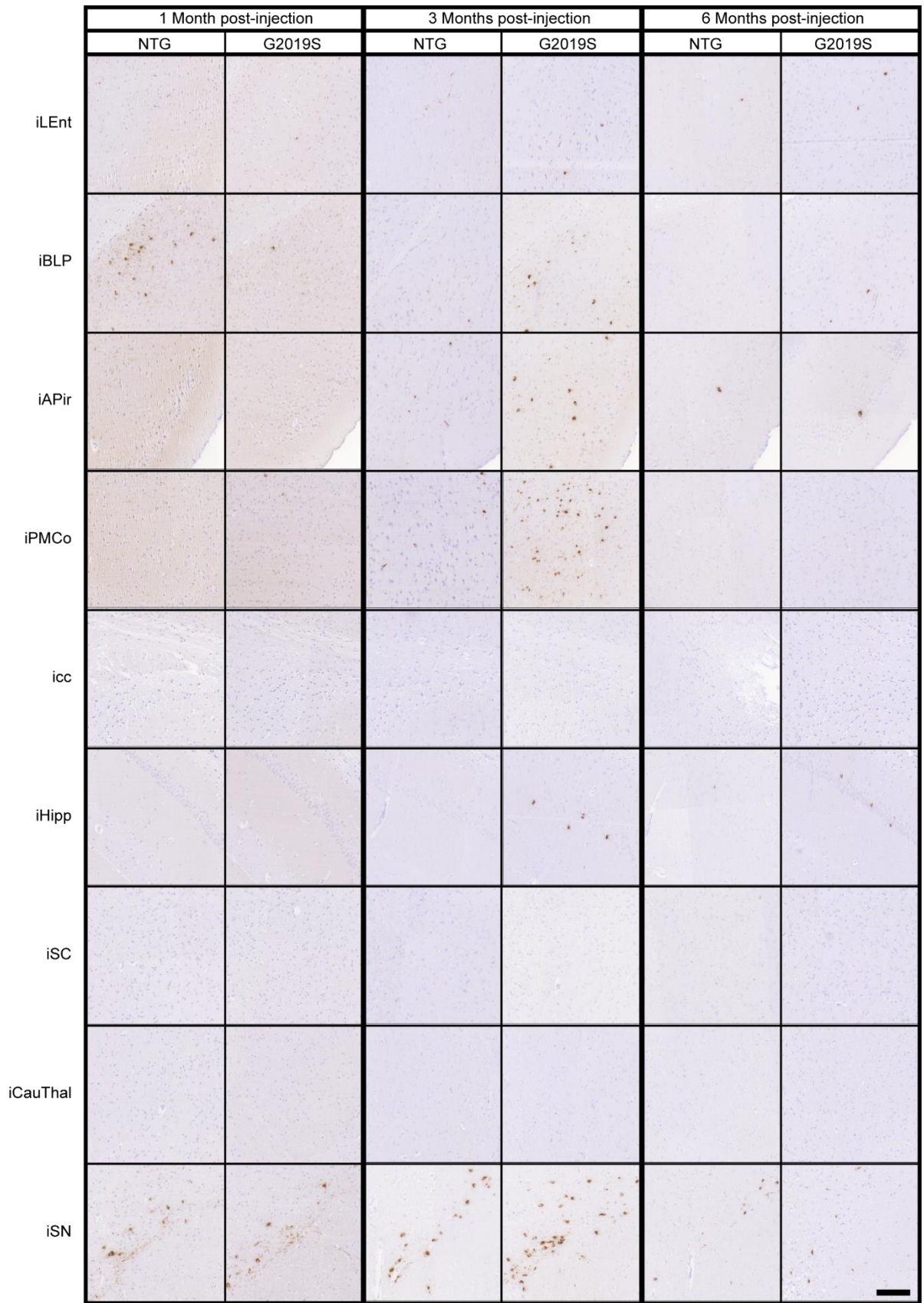
100 μm

	1 Month post-injection		3 Months post-injection		6 Months post-injection	
	NTG	G2019S	NTG	G2019S	NTG	G2019S
cVMThal						
cic						
cCPu-b						
cZI						
cTC						
cCA						
cBLA						
cBMA						

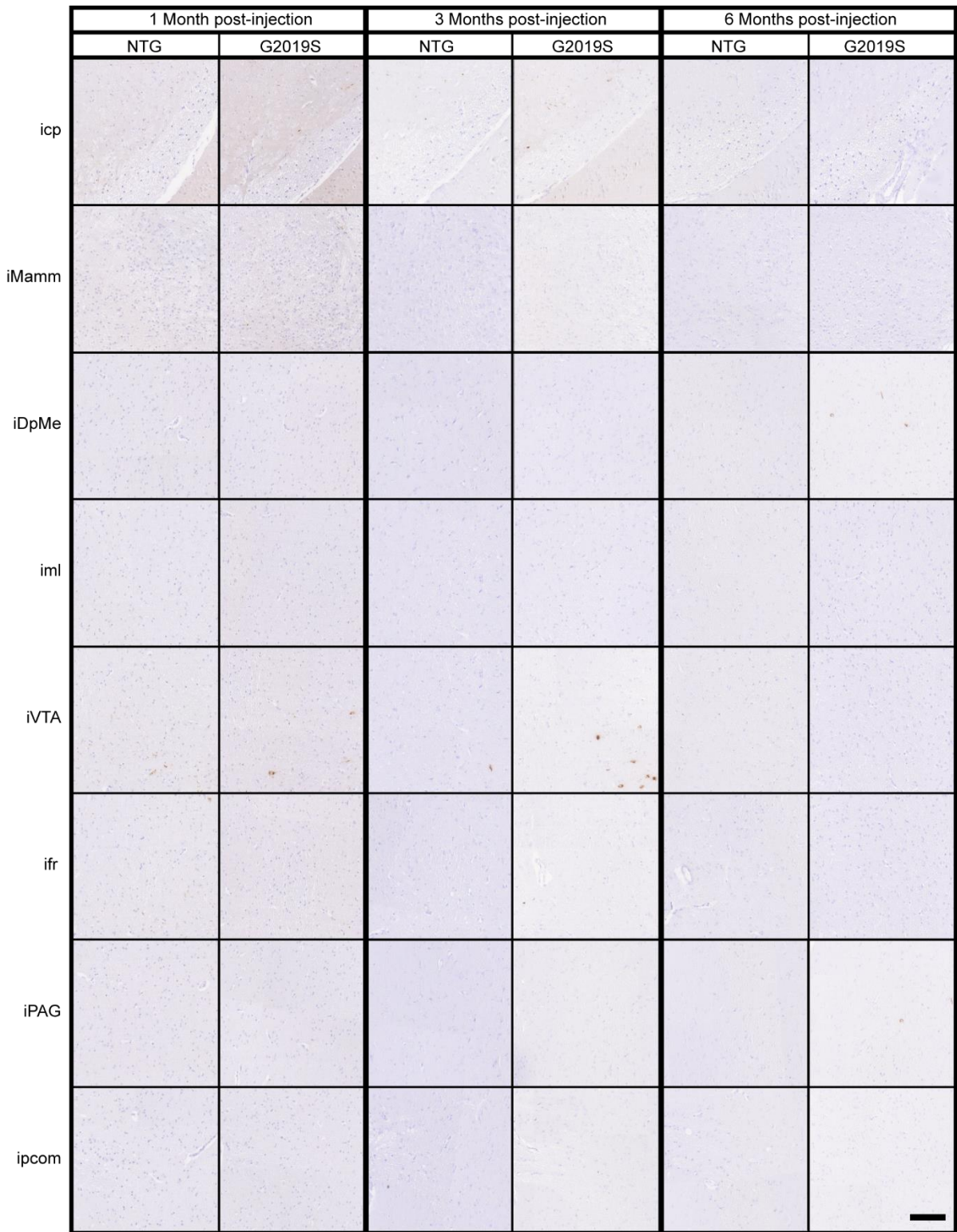
100 μm

	1 Month post-injection		3 Months post-injection		6 Months post-injection	
	NTG	G2019S	NTG	G2019S	NTG	G2019S
icc						
ccc						
iRSC-b						
iV						
iAu						
iTeA						
iEct						
iPRh						

100 μm



100 μm



100 μm

	1 Month post-injection		3 Months post-injection		6 Months post-injection	
	NTG	G2019S	NTG	G2019S	NTG	G2019S
cRSC-b						
cV						
cAu						
cTeA						
cEct						
cPRh						
cLEnt						
cBLP						
cAPir						

100 μm




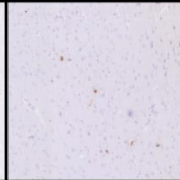


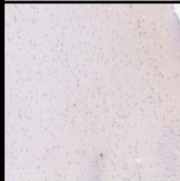
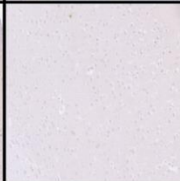


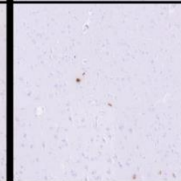
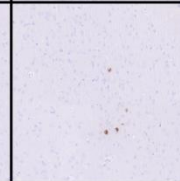
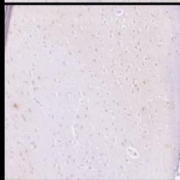
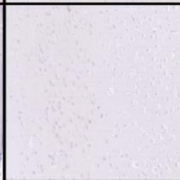

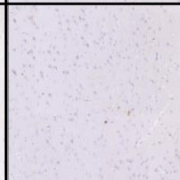

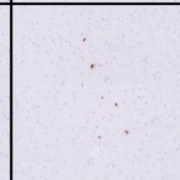

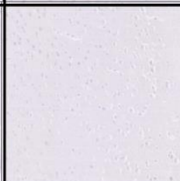


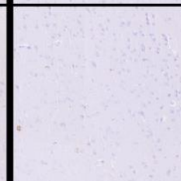
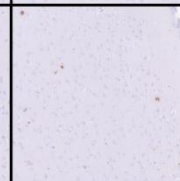

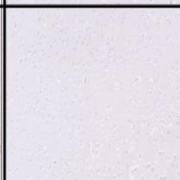
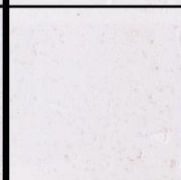

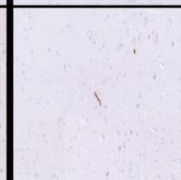


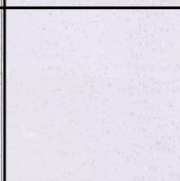
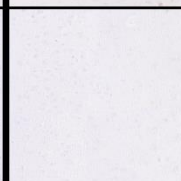
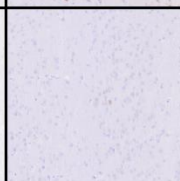

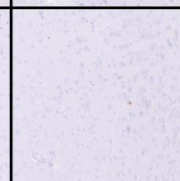

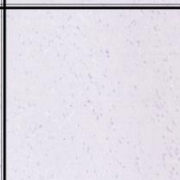
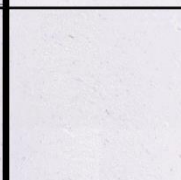

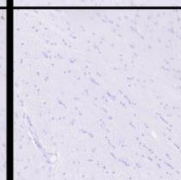

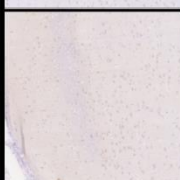
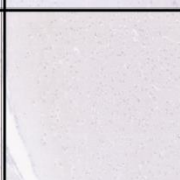





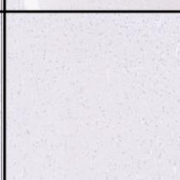
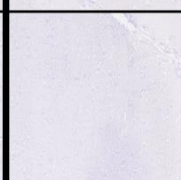
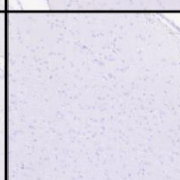

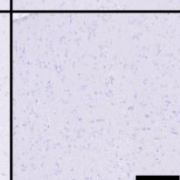


	1 Month post-injection		3 Months post-injection		6 Months post-injection	
	NTG	G2019S	NTG	G2019S	NTG	G2019S
cPMCo						
ccc						
cHipp						
cSC						
cCauThal						
cSN						
ccp						
cMamm						
cDpMe						

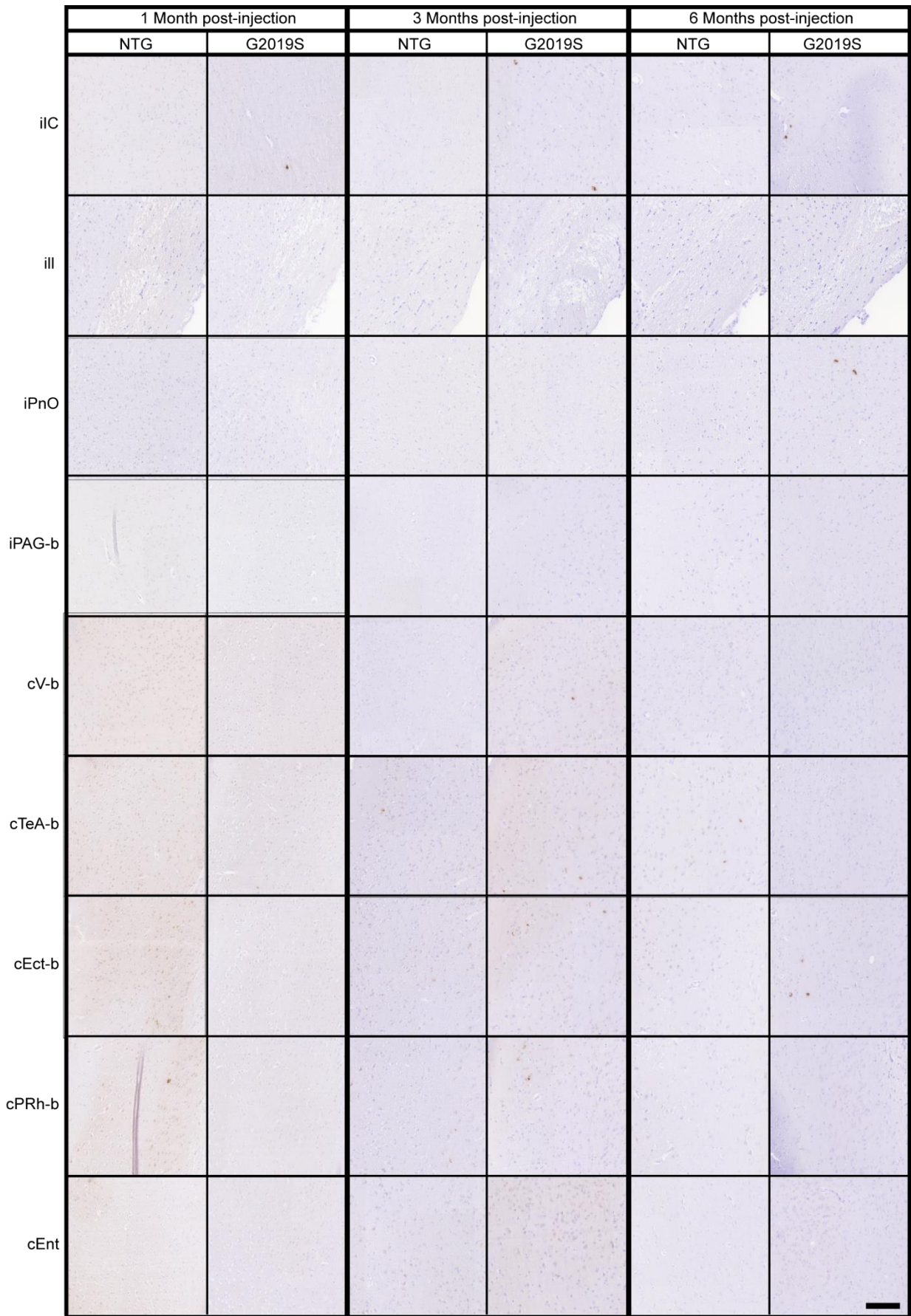
100 μm

	1 Month post-injection		3 Months post-injection		6 Months post-injection	
	NTG	G2019S	NTG	G2019S	NTG	G2019S
cml						
cVTA						
cfr						
cPAG						
cPCom						
iSum						
cSum						
ixscp						
cxscp						

100 μm

	1 Month post-injection		3 Months post-injection		6 Months post-injection	
	NTG	G2019S	NTG	G2019S	NTG	G2019S
iV-b						
iTeA-b						
iEct-b						
iPRh-b						
iEnt						
iPS						
idhc						
iRSA						
iSuC						

100 μm



100  $\mu$ m

